Geophysical Journal International

Geophys. J. Int. (2021) **224,** 2016–2027
Advance Access publication 2020 November 19
GJI Geodynamics and Tectonics

doi: 10.1093/gji/ggaa560

Present GPS velocity field along 1999 Izmit rupture zone: evidence for continuing afterslip 20 yr after the earthquake

Seda Özarpacı [1], Uğur Doğan [1], Semih Ergintav,[2] Ziyadin Çakır,[3] Alpay Özdemir,[1] Michael Floyd [4] and Robert Reilinger[4]

[1] *Department of Geomatic Engineering, Yildiz Technical University,* 34220 *Istanbul, Turkey. E-mail: dogan@yildiz.edu.tr*
[2] *Department of Geodesy, Kandilli Observatory and Earthquake Research Institute, Bogazici University,* 34684 *Istanbul, Turkey*
[3] *Department of Geology, Istanbul Technical University,* 34469 *Istanbul, Turkey*
[4] *Department of Earth, Atmospheric and Planetary Sciences, Massachusetts Institute of Technology, Cambridge,* 02139 *MA, USA*

Accepted 2020 November 17. Received 2020 October 16; in original form 2020 February 19

SUMMARY

In order to better assess earthquake hazards, it is vital to have a better understanding of the spatial and temporal characteristics of fault creep that occur on ruptured faults during the period following major earthquakes. Towards this end, we use new far-field GPS velocities from continuous stations (extending ∼50–70 km from the fault) and updated near-fault GPS survey observations, with high temporal and spatial density, to constrain active deformation along the M_w7.4, 1999 Izmit, Turkey Earthquake fault. We interpret and model deformation as resulting from post-seismic afterslip on the coseismic fault. In the broadest sense, our results demonstrate that logarithmically decaying post-seismic afterslip continues at a significant level 20 yr following 1999 Earthquake. Elastic models indicate substantially shallower apparent locking depths at present than prior to the 1999 Earthquake, consistent with continuing afterslip on the coseismic fault at depth. High-density, near-fault GPS observations indicate shallow creep on the upper 1–2 km of the coseismic fault, with variable rates, the highest and most clearly defined of which reach ∼12 mm yr^{-1} (10–15 mm yr^{-1}, 95 per cent c.i.) near the epicentre between 2014–2016. This amounts to ∼half the long-term slip deficit rate.

Key words: Creep and deformation; Satellite geodesy; Seismic cycle; Earthquake hazards.

1 INTRODUCTION

The right-lateral, strike-slip North Anatolian Fault (NAF) is one of the longest and most active strike-slip faults in the world. Starting from the Karliova Triple Junction in eastern Turkey, the NAF runs westward roughly parallel to and about 100 km inland from the Black Sea coast, and extends across the North Aegean Sea to central Greece (Ambraseys 1970; Şengör *et al.* 2005; Zabcı 2019). The 1939, M_w7.8, Erzincan Earthquake initiated the westward migration of a sequence of major earthquakes on the NAF (Barka *et al.* 1996; Stein *et al.* 1997; Nalbant *et al.* 1998; Şengör *et al.* 2005; Lorenzo-Martín *et al.* 2006). The last of this sequence was the 1999, M_w7.4 Izmit Earthquake (Fig. 1). The 1912 Ganos Earthquake (Fig. 1, M_w7.4) bounds the Marmara region to the west; these events bracket the 'Marmara Seismic Gap'. The Marmara Seismic Gap and, indeed, the Izmit Earthquake segment were identified prior to the Earthquake (Toksöz *et al.* 1999), so a substantial GPS network including continuous and survey mode observations was developed prior to the Earthquake (Straub *et al.* 1997; McClusky *et al.* 2000). These early and continuing geodetic observations, and subsequent monitoring with GPS and InSAR, make the 1999 Izmit Earthquake one of the best observed, well-studied earthquakes in the world (e.g. Toksöz *et al.* 1999; Armijo *et al.* 2000; Reilinger *et al.* 2000; Wright *et al.* 2001; Barka *et al.* 2002; Bürgmann *et al.* 2002).

Post-seismic deformation for the 1999 Izmit Earthquake has been reported and investigated by a number of researchers (Ergintav *et al.* 2002, 2007, 2009, 2014; Hearn *et al.* 2002; Çakır 2003; Çakır *et al.* 2003). Interpretations and modelling included both viscoelastic relaxation of the lower crust and/or upper mantle (e.g. Hearn *et al.* 2009; Wang *et al.* 2009), and afterslip on and adjacent to the coseismic fault (e.g. Ergintav *et al.* 2009; Çakır *et al.* 2012; Hussain *et al.* 2016a; Aslan *et al.* 2019). Here, we consider only afterslip based on observations of continuing surface creep and the narrow zone of strain surrounding the coseismic fault (e.g. Ergintav *et al.* 2014; Yamasaki *et al.* 2014).

GPS and Interferometric Synthetic Aperture Radar (InSAR) studies showed that surface creep along the 1999 Izmit Earthquake rupture began after the coseismic displacement as afterslip decaying rapidly and approaching what was interpreted as steady-state creep (Çakır *et al.* 2012). Using additional InSAR data, Hussain *et al.* (2016a) reported aseismic slip along the Izmit rupture that reached the surface, with a maximum rate of 11 ± 2 mm yr^{-1} near the city

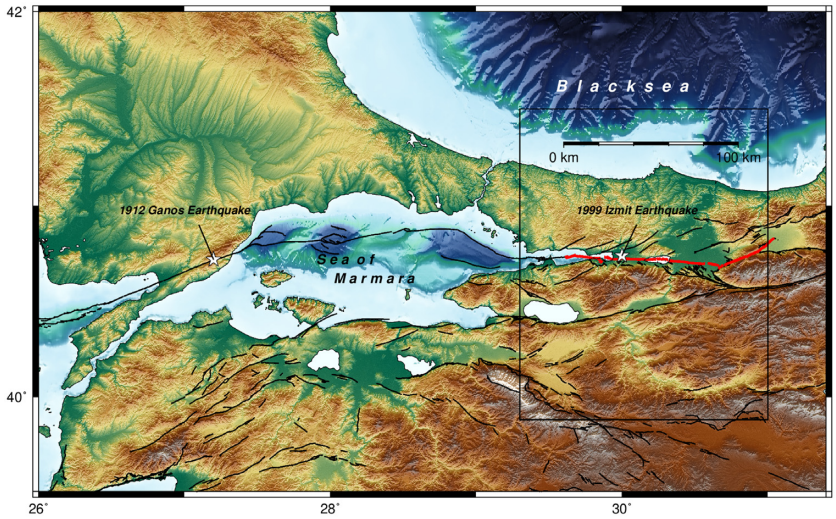

Figure 1. Marmara region with the study area in rectangle. Stars show the 1912 Ganos and the 1999 Izmit earthquake locations from west to east. Red thick lines shows the 1999 Izmit earthquake surface trace and the black thin lines shows active faults (Emre *et al.* 2013).

of Izmit between 2002 and 2010. Using Sentinel 1A/B Terrain Observation by Progressive Scans (TOPS) images between 2014 and 2017, GPS observations and creepmeter data, Aslan *et al.* (2019) confirmed that shallow creep along the Izmit rupture is still ongoing at an estimated rate of ∼8 mm yr^{-1}. They showed that creep occurs both as a steady process and by episodic accelerated slip events.

The accuracy in earthquake probability calculations (e.g. Parsons 2004) is directly related to the amount of strain accumulated on the fault. Aseismic creep along a fault complicates estimates of the elastic strain and earthquake potential on the fault (Bürgmann *et al.* 2000). Thus, estimation of seismic potential of faults depends on understanding fault coupling (Bohnhoff *et al.* 2017). With the help of geodetic techniques, it is possible to constrain spatiotemporal evolution of slip (Avouac 2015; Aslan *et al.* 2019).

In this paper, we provide a recent regional velocity field around the Izmit coseismic rupture using GPS data collected 13–20 yr following the Earthquake. These observations are used to constrain fault-scale estimates of strain accumulation (slip rate and apparent fault locking depth) on the central Izmit coseismic fault using simple, 2-D elastic models. Comparisons with pre-earthquake estimates of strain accumulation demonstrate that the Izmit fault continues to experience post-seismic effects. We further use near-fault GPS observations between 2014 and 2016 to investigate the temporal and spatial evolution of across-fault displacements. We use elastic models to estimate shallow creep rate and apparent locking depth and show that the largest afterslip is occurring near the Izmit Earthquake epicentral region. We combine our models to quantify both deep and shallow post-seismic behaviour. Finally, we extend a near-fault GPS baseline observed frequently since before the 1999 earthquake and confirm that shallow afterslip on this section of the Izmit fault is well modelled by logarithmic decay since the time of the earthquake.

2 GPS DATA AND PROCESSING

GPS velocities between 2013 and 2020 are determined at 49 locations (Fig. 2). Of these, 30 are measured with survey mode (sGPS) as profiles oriented perpendicular to the fault, and the rest being continuous stations (cGPS). As indicated in Table S1 in the Supporting Information that provides details of the GPS observations, velocities are determined over different time spans. Near-field sGPS campaigns were conducted five times and twice a year around May and October between 2014 and 2016 in order to minimize annual systematic errors. One further campaign was completed in 2019 May only for SMAS and SISL sites in order to extend earlier observations and observe the latest deformation in the region. All the observations were collected in sessions of at least 10 hr using dual-frequency GPS receivers and geodetic antennas. By measuring these stations close to the fault (from a few metres to 10 km distance), we aimed to determine the temporal and spatial variation of any ongoing, aseismic creep. The cGPS data were obtained from the National Permanent Network in Turkey (TUSAGA-Active), Kocaeli General Directorate of Water and Sewerage Administration (ISU), Sakarya General Directorate of Water and Sewerage Administration (SASKI) and Cayirova Municipality. Installation of these stations was conducted at different times. TUSAGA-Active stations have the longest period data between 2013 and 2020. Three stations (ISUU, GEBZ and EREN) of ISU are the closest continuous stations to the fault. Although their duration is short (about 2.5 yr), they are important due to their proximity to the fault and compatibility with other observations.

The GPS data were processed using the GAMIT/GLOBK (V10.7) GNSS software (Herring *et al.* 2018) in three stages (Dong *et al.* 1998; McClusky *et al.* 2000; Reilinger *et al.* 2006). In the first stage, we use the GAMIT software to analyse phase measurements from each day to estimate coordinates of each station. In the second stage, using the GAMIT output h-files that contain ambiguity-fixed, loosely constrained network solutions, we produce time-series of daily coordinates of each station. After this step, we inspect for outliers and we analyse the time-series from each station to estimate trend and characterize temporally correlated noise characteristics, including the estimation of seasonal (annual and semi-annual) effects. As the last stage, we use a Kalman filter to estimate velocities with respect to Eurasia for each GPS site, using the equivalent random-walk noise estimated from the time-series in the previous step to maintain more realistic velocity uncertainties (Floyd & Herring 2020). Processing of the survey sites is the same as the continuous sites in the first two steps. At the third step, we used the

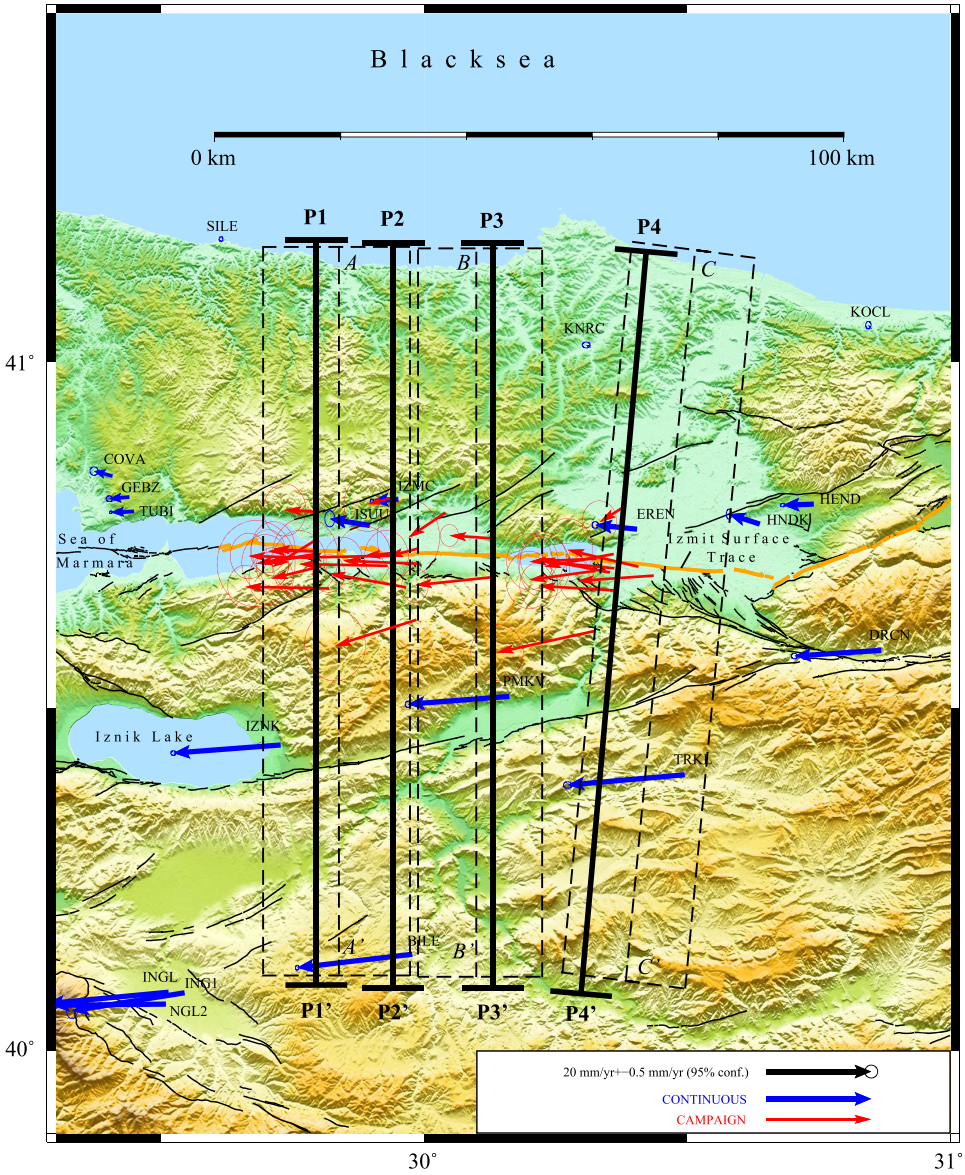

Figure 2. Long profiles perpendicular to the fault along the 1999 Izmit rupture zone. Also shown are cGPS (blue vectors) and sGPS (red vectors) velocities with 95 per cent confidence ellipses relative to Eurasia, 1999 Izmit rupture (orange lines) and active faults (black lines, Emre *et al.* 2013).

median random-walk noise estimated from the time series of continuous stations for the survey sites to make velocity uncertainties more realistic. The horizontal velocity field is given with uncertainties for continuous and survey GPS stations in Table S1 in the Supporting Information, and Fig. 2 illustrates the velocity field of the region with blue and red arrows for cGPS and sGPS stations, respectively.

3 MODELLING

In this paper, we neglect possible effects of broad viscoelastic deformation, because we focus on near-field deformation, and consider only models of strain accumulation and release on the primary Izmit coseismic fault. For the near-fault observations that are sensitive to near surface fault processes, this approach finds support from creep meter observations that demonstrate surface fault creep and InSAR observations that indicate a sharp change across the surface fault (e.g. Aslan *et al.* 2019).

We use simple 2-D models (Savage & Burford 1973) to estimate the slip rates near each profile location. This approach provides an opportunity to compare model estimates with previous studies because the locations of the profiles are identical (Çakır *et al.* 2012; Hussain *et al.* 2016a; Aslan *et al.* 2019). We decided not to use 3-D modelling, which estimates slip variability along fault and at depth a regular grid interval because the near-field data are poorly distributed along the fault trace, and 3-D modelling would necessarily smear the estimated slip between the location of our fault-crossing profiles.

To correct profile velocities for the rotation of the Anatolian region (McClusky *et al.* 2000), we used well-determined velocities far from the fault (Fig. S1, Supporting Information) to estimate a regional Euler vector for a broad area south of the Izmit coseismic fault.

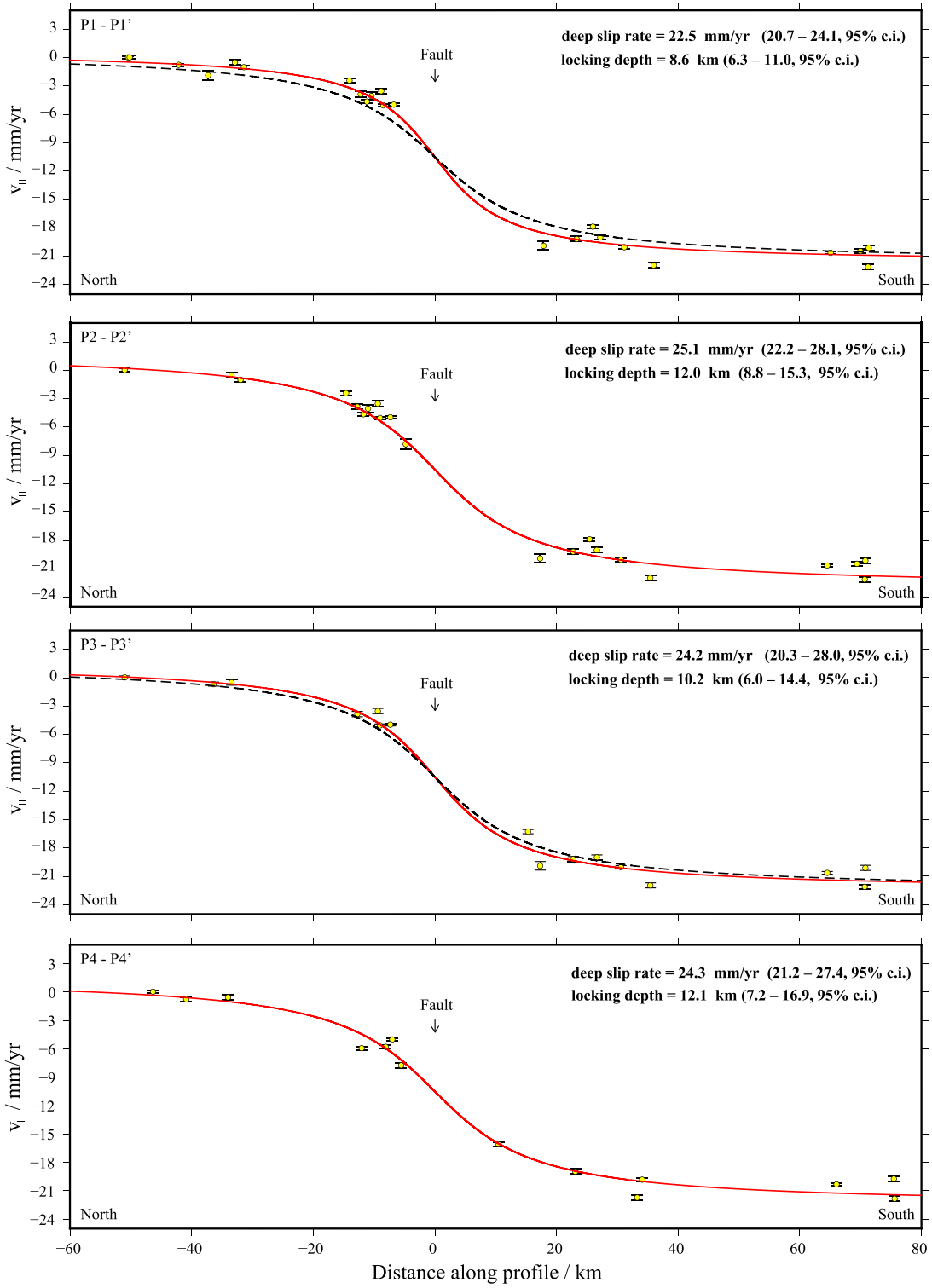

Figure 3. Long profiles perpendicular to the fault along the 1999 Izmit rupture. Blue points are the fault–parallel GPS continuous station velocities and their 95 per cent confidence interval. Red line is a least-squares fit to the fault-parallel velocities using a simple elastic dislocation model that estimates deep slip rate and the locking depth. The black dashed line is for a fault which has 12 km locking depth.

The long profiles used for far-field velocity estimation extend 70–75 km south of the fault, and 50 km north (Fig. 2). The short profiles are ∼30 km long and 10 km wide (Fig. 4), and follow roughly the same paths as the long profiles.

Shallow and deep slip rates are estimated in two stages. First, near-fault velocities are ignored and deep slip and locking depth are estimated from the far-field observations. These estimates are fixed and shallow slip rates are estimated from the near-fault profiles.

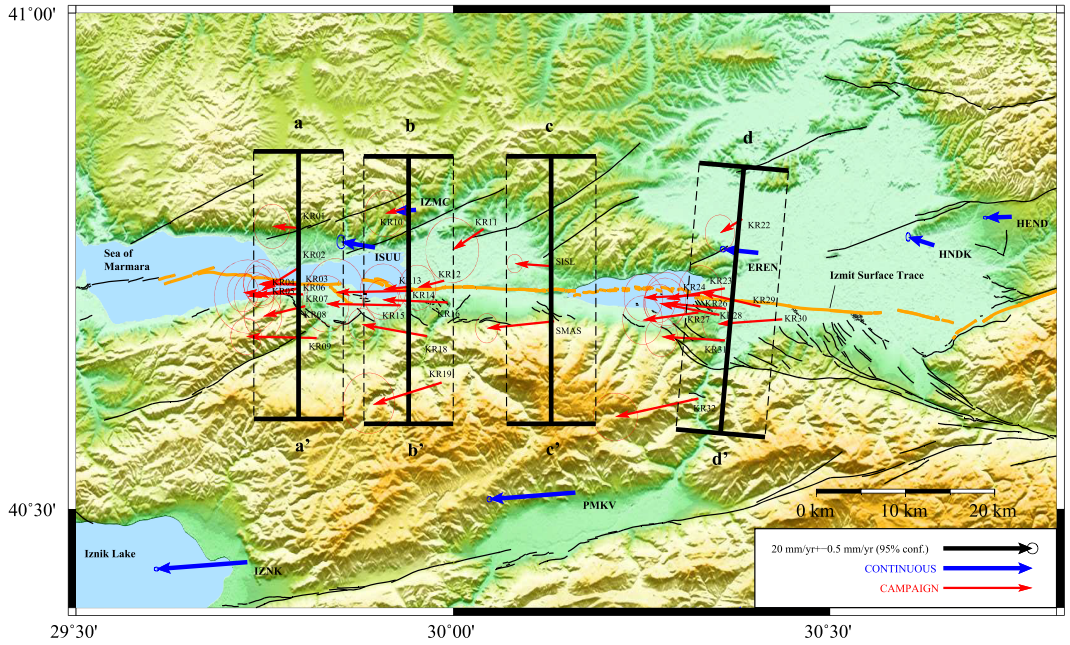

Figure 4. Map of the Izmit rupture (orange lines) and active faults (black lines, Emre *et al.* 2013) with GPS velocities from campaign measurements (red vectors) that were measured between 2014 and 2016 every six months, and selected continuous stations (blue vectors) with 95 per cent confidence ellipses relative to Eurasia. (See Table S1 in the Supporting Information for observation periods of each station.)

This approach minimizes the correlation between shallow and deep slip rates (and their depths) in the classical approach (Hussain *et al.* 2016a; Aslan *et al.* 2019).

3.1 Slip rate estimates from elastic modelling of fault-parallel far-field velocities

Estimates of deep slip rates and fault locking depth were determined by fitting our GPS velocities with a simple dislocation model in an elastic half-space (Savage & Burford 1973; Savage 1990) consisting of the far-field velocity V and the locking depth D (Savage & Burford 1973). An accurate estimate of the far-field velocity, resulting from fault slip rate, requires GPS velocity data more than several locking depths away from the fault (>50km), while an accurate estimate of the locking depth requires a high density of GPS velocity data within one-half locking depth of the fault (Smith-Konter *et al.* 2011).

The 2-D model velocity profile across the locked fault zone is given by

$$v_{||}(x) = \frac{V}{\pi}\arctan(\frac{x}{D}) + c \qquad (1)$$

where V is the far-field velocity (plate rate), x is the horizontal fault-perpendicular distance, D is the locking depth and the coefficient c defines the vertical origin of the curve (Savage & Burford 1973). Parameter V controls the amplitude of the arctangent whereas its curvature varies inversely to D. A nonlinear least-squares procedure that takes into account velocity uncertainties was used to derive parameters V, D and c and their formal uncertainties. Geodetically determined deep slip rates along the 1999 Izmit rupture vary between 22.5 and 25.1 mm yr^{-1}, with a mean of 24 mm yr^{-1} and a standard deviation of 1.4 mm yr^{-1}, and locking depths ranging from 8.6 to 12.1 km with a mean of 10.7 km and a standard deviation of 1.8 km. Uncertainties (2σ) in slip rates and locking depth are typically 0.9 to 1.9 mm yr^{-1} and 1.2 to 2.4 km, depending on the density and quality of nearby geodetic observations (Fig. 3).

3.2 Slip rate estimates from elastic modelling of fault-parallel near-field velocities

We now model fault-parallel velocities as the sum of two separate processes. The first process, described above, considers strain accumulation on the fault as a whole due to deep, interseismic strain accumulation. Additionally, we estimate fault creep on the shallow part of the fault. The displacement velocity (v) generated by the aseismic slip occurring on shallow and deep faults at a distance perpendicular to the fault (x) is calculated by the formula;

$$v_{||}(x) = \frac{v_d}{\pi}\arctan(\frac{x}{d_1}) + v_c\left[\frac{1}{\pi}\arctan(\frac{x}{d_2}) - H(x)\right] + o \qquad (2)$$

where v_c is the surface creep velocity, v_d is the interseismic rate, d_2 is the lower depth of the shallow creep zone, d_1 is the locking depth (depth of the seismogenic zone), o is the velocity offset and H is Heaviside function.

As mentioned above, it is difficult to isolate the shallow aseismic slip rate from long profiles, so we first determined the interseismic rate v_d and locking depth d_1 in the first term of eq. (2), using the fault-parallel component of far-field velocities described in Section 3.1. Subsequently, to estimate aseismic slip on the shallow coseismic fault, we fix the values for deep slip rate and apparent locking depth, and calculate the shallow creep rate and creep depth. Fig. 4 shows the near-fault velocities used to estimate spatial variations of aseismic slip along the Izmit rupture.

Fig. 5 shows profiles of the fault-parallel velocities along profiles $a-a$', $b-b$', $c-c$' and $d-d$' in Fig. 4. We model these profiles to estimate creep rates and depths within 95 per cent confidence intervals as given on the figure.

The largest, and best-defined offset across the fault occurs along profile $b-b$', crossing the fault near the epicentre of the 1999 earthquake, and indicating a creep rate of $\sim$ 12 mm yr^{-1} and with creep confined to within 1–2 km depth. Aseismic shallow slip decreases on the eastern and western parts of the rupture zone

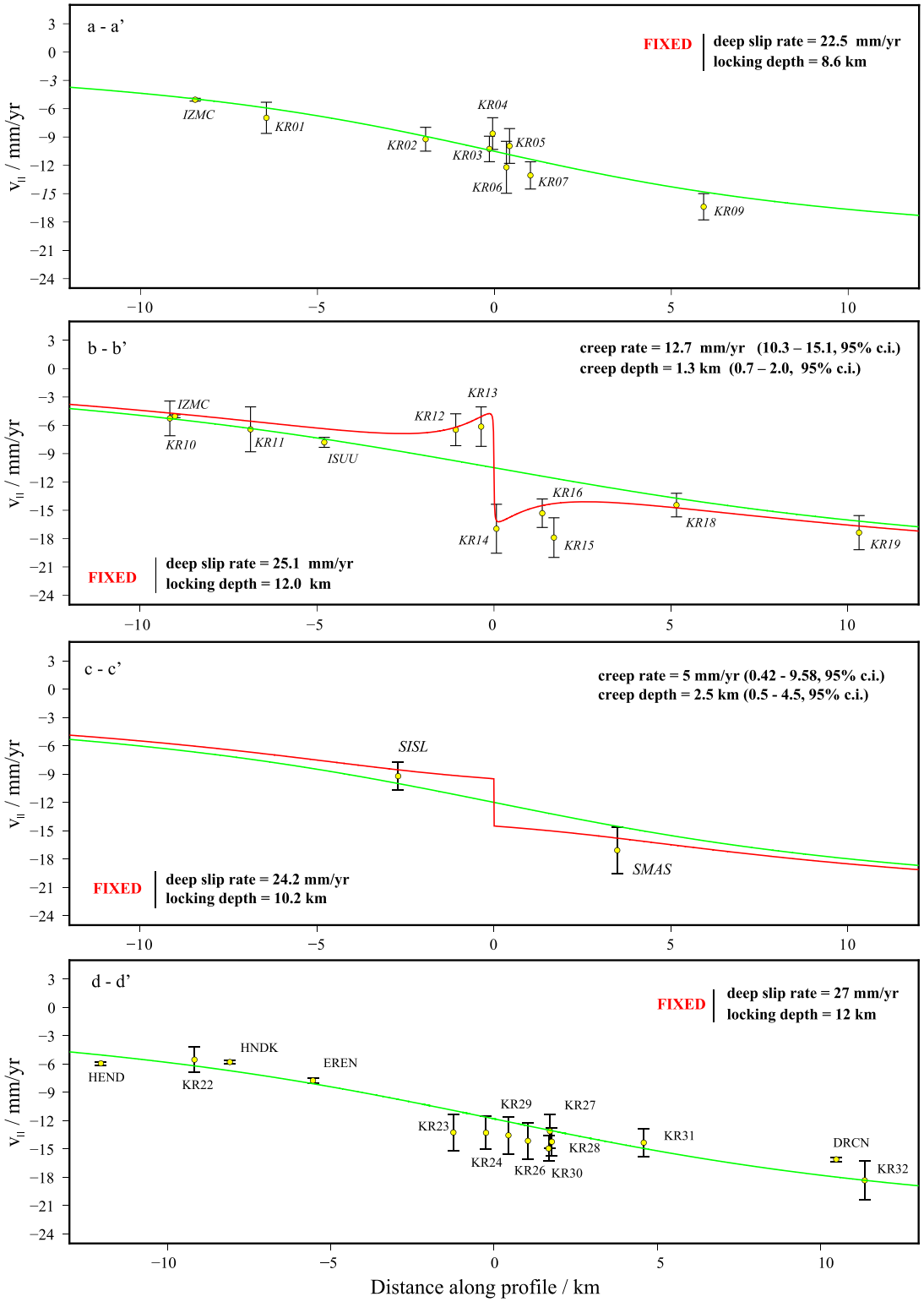

Figure 5. Profiles of fault-parallel velocities along $a - a$', $b - b$', $c - c$' and $d - d$' in Fig. 4. Yellow dots are GPS points showing the fault-parallel velocity components. Red is the best fit of elastic dislocation model with fixed deep slip rate and locking depth that we found with the long-wavelength signal, plus shallow creep. Green is the best fit to the far-field GPS observations without surface creep.

(green line with no surface creep fits the profile $a - a$' and $c - c$'). For the eastern-most profile $d - d$', the fault-parallel component of GPS velocities shows no surface creep. Profile $c - c$' suffers from insufficient survey sites. Although we fit the red line with surface creep at this profile, there are only two sites straddling the fault and the uncertainty on parameter estimates are very high.

Although sparse, the $c - c$' profile is important because of the long-term measurements crossing this section of the coseismic fault.

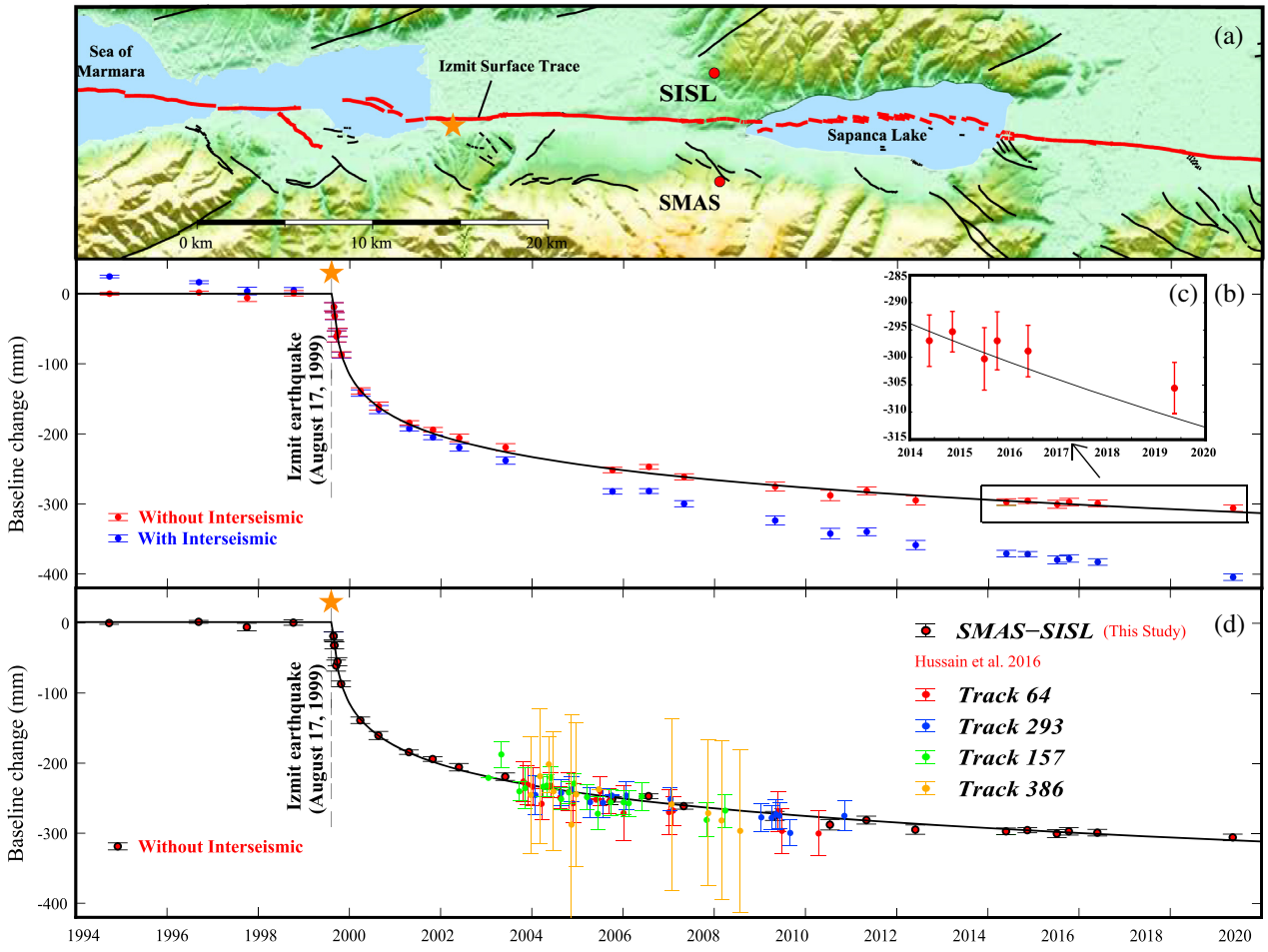

Figure 6. SMAS–SISL baseline. (a) Locations of two stations with the 1999 Izmit rupture (red lines), and active faults (black lines, Emre *et al.* 2013). (b) East–west component of the baseline change from 1994 to 2019 with coseismic offset removed. Orange star shows the time of the earthquake. Blue points are observed time-series and red values are the series after subtraction of the secular (interseismic) velocity, which was estimated using pre-earthquake site velocities (McClusky *et al.* 2000). The latest observations and the afterslip model (black curve) indicate that the afterslip of the Izmit Earthquake is still ongoing 20 yr after the earthquake. Black curve is a fit to the GPS data of the form $a + bt + c\log(1 + dt)$ (t is time in yr). The coefficients a, b, c and d inverted with a Levenberg–Marquardt inversion approach are -21.81 ± 4.1 mm, -0.35 ± 0.1 mm yr^{-1}, -48.39 ± 2.9 mm, and 17.28 ± 4.2 mm yr^{-1}, respectively. (c) The 2014–2016 campaign interseismic rate removed data that are the subject of this paper, and the last survey from these two stations, are shown in a close-up window to better illustrate ongoing post-seismic deformation. (d) The same GPS time-series including InSAR results from Hussain *et al.* (2016b).

Sites SMAS and SISL (Fig. 6a), bracket the fault ~ 3 km from the fault trace were measured before the 1999 Izmit Earthquake with a history dating back 25 yr, with frequent observations. The SMAS-SISL baseline (Fig. 6b), which was earlier reported by Çakır *et al.* (2012) who interpreted the rapid baseline change as due to post-seismic afterslip, has continued to be measured in order to extend monitoring of the temporal variations of creep on the fault. The updated results for the change in baseline length for the SMAS and SISL baseline are shown in Fig. 6(c).

4 DISCUSSION

The first fault creep results for the 1999 Izmit surface rupture were reported by Çakır *et al.* (2012). They modelled creep rates with fault-parallel velocities using both InSAR and GPS. Subsequent studies such as Hussain *et al.* (2016a), and Aslan *et al.* (2019) used InSAR data with a similar approach to investigate temporal and spatial variations in fault creep. In this study, we update GPS position and velocity estimates, again using the same methods in order to compare all results. As in our study, both Hussain *et al.* (2016a) and Aslan *et al.* (2019) identified aseismic slip in the epicentral region that had a larger magnitude than on other segments along the Izmit earthquake rupture. We used the same profiles as Aslan *et al.* (2019) (i.e. P1–P1' to P4–P4' in Fig. 2). In Fig. 2, the profiles used in Hussain *et al.* (2016a) approximately coincide with A–A' to C–C. Both studies report that after slip decreases to the east. In our study, the profile traversing the fault close to the epicentre has the greatest creep rate. Hussain *et al.* (2016a) reported 11 ± 2 mm yr^{-1} close to Izmit City (near the epicentre) between 2002 and 2010 and Aslan *et al.* (2019) report a creep rate of 8 ± 1 mm yr^{-1} between 2011 and 2017 (Fig. 7). Our updated analysis gives a creep rate near the epicentre of the earthquake of ~12.7 mm yr^{-1} (10.3–15.1, 95 per cent c.i.) between 2014 and 2016. Our result indicates rapid ongoing shallow creep, but is not sufficient to identify any change in the creep rate with time given

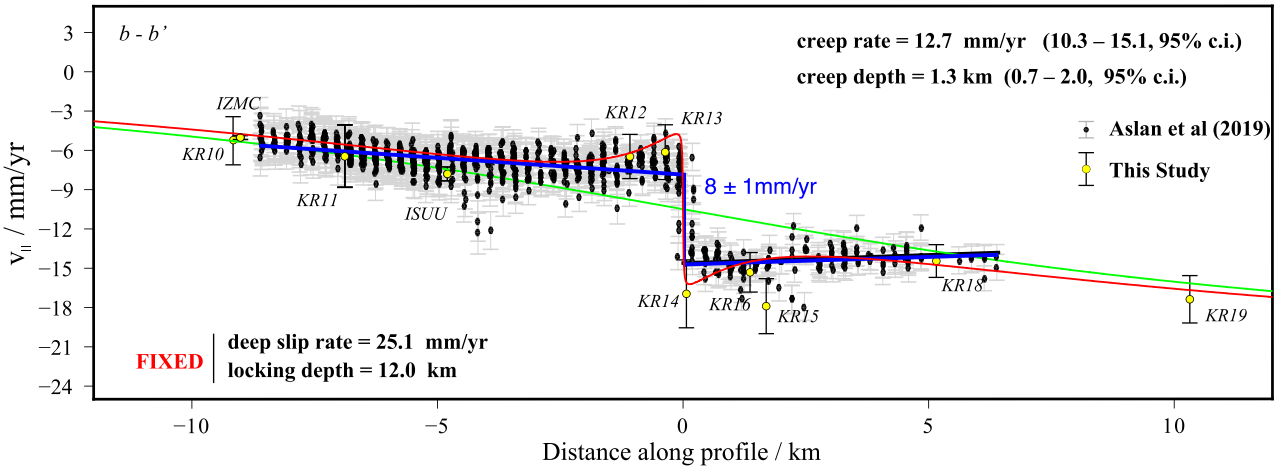

Figure 7. Profile of fault-parallel velocities along *b*–*b*' in Fig. 4 with Aslan *et al.* (2019). Yellow dots are GPS points showing the fault-parallel velocity components. Red is the best fit of elastic dislocation model with fixed deep slip rate and locking depth that we found with the long-wavelength signal, plus shallow creep. Green is the best fit to the far-field GPS observations without surface creep. Blue fit is from Aslan *et al.* (2019) creep results.

observational uncertainties and indications that surface creep can occur episodically (Aslan *et al.* 2019). To the east of Lake Sapanca, Hussain *et al.* (2016a) found the slow slip to be about 2 mm yr^{-1} (0–5, 95 per cent c.i.) between 2002 and 2010, and Aslan *et al.* (2019) calculated slow slip in this region of about 1.3 mm yr^{-1} (±0.3, 95 per cent c.i.), in agreement within uncertainties with our findings.

Hussain *et al.* (2016a) also used GPS baseline time series of SMAS-SISL from Çakır *et al.* (2012) combined with their own InSAR results between 2002 and 2010. They estimated and adjusted the observations for pre-seismic and coseismic displacements and interseismic strain, and interpreted the remaining signal as shallow fault creep. We updated this same baseline adding new GPS measurements (Fig. 6d), and confirm that the afterslip rate continues to decrease. Assuming their interpretation of afterslip is correct, the 1999 Izmit Earthquake triggered one of the longest lasting afterslip episodes recorded on a strike-slip fault.

In addition to continuously decreasing slip rates, InSAR and creepmeter time-series reveal episodic creep events (Aslan *et al.* 2019). To confirm this observation, and to further constrain temporal and spatial variations of creep, we calculate the east cumulative motions for GPS survey sites near the 1999 epicentre by summing the absolute values of the east residuals of the GPS campaign data (Fig. 8a). (In Fig. 8a, note that sites north of the fault consistently move eastward, and those to the south move westward.) In addition to the approximately steady offsets, the cumulative time-series indicate a consistent increase in site offsets between the third and fourth campaigns between 2015 July and August (the grey band in Figs 8a–c); providing support for the creep event reported by creep event reported by Fig. 8(b). The observed 2015 September increase in site motions is most pronounced for site KR14, just to the south and closest to the 1999 epicentre and fault break. KR13 is north of the fault and KR14 is south of the fault, therefore the maximum velocity difference occurs between these sites and very near the epicentre of the 1999 Izmit Earthquake. While there is no local seismic network in the region, the ISC earthquake catalogue (International Seismological Centre 2018; Bondár & Storchak 2011) lists no earthquakes between these campaigns with sufficient magnitude to account for the large amplitude of the observed offsets (Fig. 8e), indicating fault creep occurred aseismically.

To investigate how close the fault is to its pre-earthquake state of strain accumulation, in Fig. 9 we compare our results with the cross-fault velocities estimated by McClusky *et al.* (2000) using only pre-earthquake GPS observations (see Fig S2, Supporting Information), as well as with the Izmit earthquake fault crossing velocity profile reported by Ergintav *et al.* (2014). We compare fault-parallel components of the velocities with our profile P2–P2'. As indicated in the figure, the apparent locking depth estimated from our simple elastic models remains significantly shallower 20 yr after the earthquake (12 versus 21 km), clearly indicating ongoing post-seismic deformation that we attribute to afterslip.

Ergintav *et al.* (2014) estimated interseismic velocities using pre- and post-earthquake observations by attempting to remove post-seismic deformation and coseismic offsets for the 1999 Earthquake. While far-field slip rates agree well between all three results, the shallow apparent locking depth in Ergintav *et al.* (2014) indicate post-seismic transients were not fully removed.

Attribution of locking depth estimated from our elastic models to a discrete boundary is not realistic; more likely there is a transition between the upper locked portion of a fault and its deeper creeping part. It is nevertheless clear that the velocity gradient near the fault along the profiles has changed over time. A steeper velocity gradient is possibly due to shallowing of the transition between shallow locking and deep slip, as in the Savage & Burford (1973) model. But the apparent shallow locking depth could also result from aseismic slip at various depths on the fault, or the whole fault. In either case, the decreased locking depth for the recent profile compared to that of McClusky *et al.* (2000), indicates that fault healing for the broad coseismic fault following the Izmit Earthquake continues at present.

As shown in Figs 5 and 6, post-seismic effects that we attribute to ongoing afterslip contribute to near-field deformation. As shown in Fig. 6, after removing steady interseismic strain accumulation, the cumulative offset of the east component of the baselines measured for 20 yr after the 1999 Izmit Earthquake reaches nearly 30 cm (this is approximately 10 per cent of the coseismic offset, which was ∼3 m between SISL and SMAS), with a present-day velocity of approximately 2.5 mm yr^{-1}, or about 10 per cent of the geological fault slip rate. The low level of seismic activity along the Izmit coseismic rupture, indicates that fault creep occurs predominantly aseismically (see Fig. 8e for seismic activity in the region).

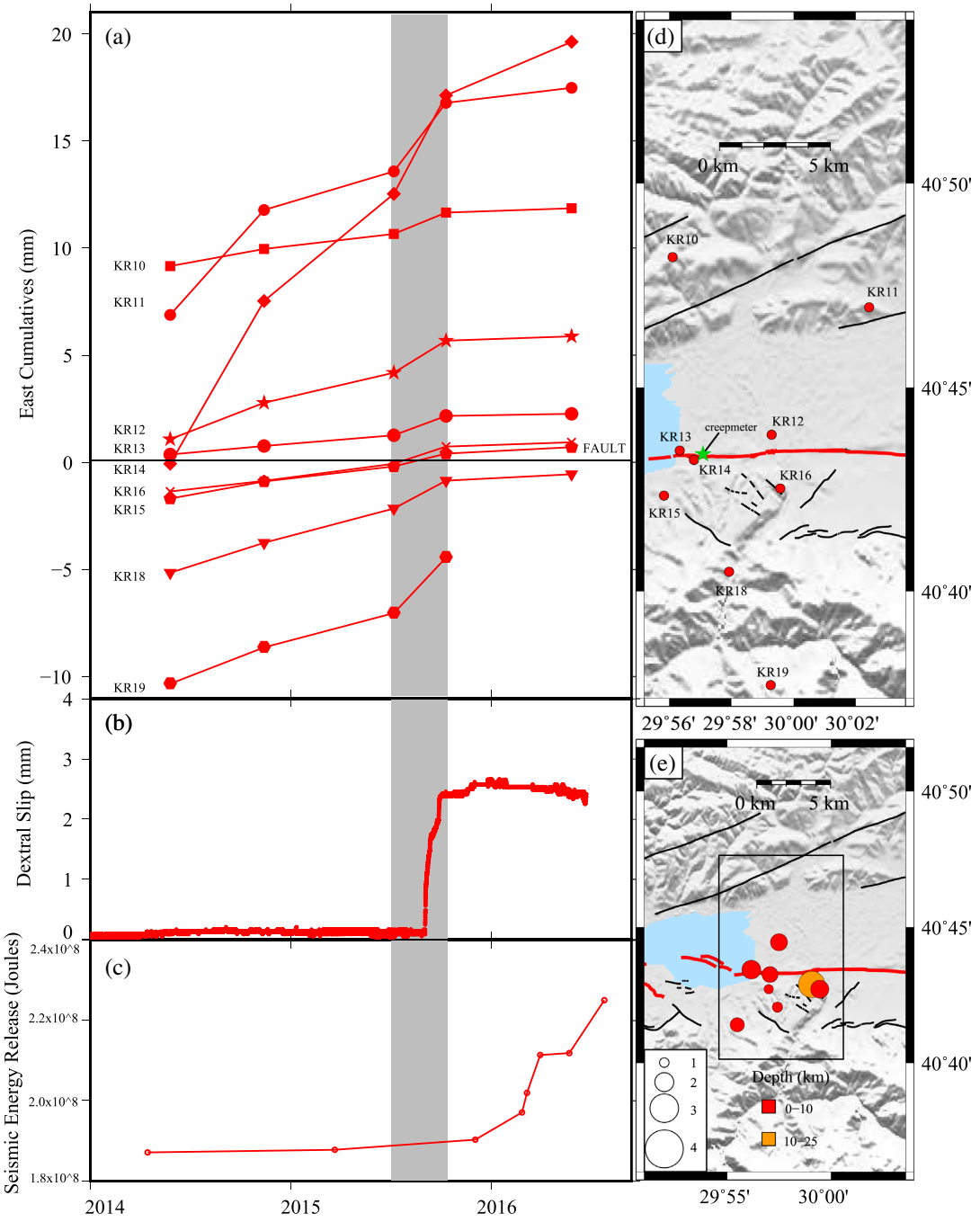

Figure 8. (a) East cumulative displacements of the absolute residual data of five GPS campaigns along profile *b*–*b*' in Figs 4 and 5 (see the text for discussion). Note that the first values of the east component are arranged according to the location of each station's distance from the coseismic fault. Note also that due to the inverted offset scale south of the fault, positive slopes indicate westward motion. (b) Dextral slip from creepmeter data (from Aslan *et al.* 2019), (c) energy release of the earthquakes in the campaign time in the rectangle (E) (International Seismological Centre 2018), (d) Survey stations along *b*–*b*', active faults (black lines, Emre *et al.* 2013) and (e) Earthquakes between 2014 and 2016, according to the ISC earthquake catalogue (International Seismological Centre 2018).

The mechanism of aseismic, shallow creep on strain accumulation on the Izmit fault segment, and adjacent segments of the NAF is not clear. One interpretation is that shallow afterslip results from continuing strain release as slip on the shallow part of the fault catches up to the larger coseismic offsets that characterized the deeper parts of the fault (e.g. Reilinger *et al.* 2000; Feigl *et al.* 2002). In this case, shallow afterslip does not contribute substantially to increased stress that would advance the fault towards failure. Our observations of shallow slip confined to the upper few kilometres is consistent with this interpretation. However, the present-day shallow locking depth for the Izmit fault as a whole (∼12 km) compared to the locking depth estimated prior to the 1999 Izmit Earthquake (∼21 km) indicates that substantial aseismic afterslip likely continues at greater (mid- to lower crustal) depths on the

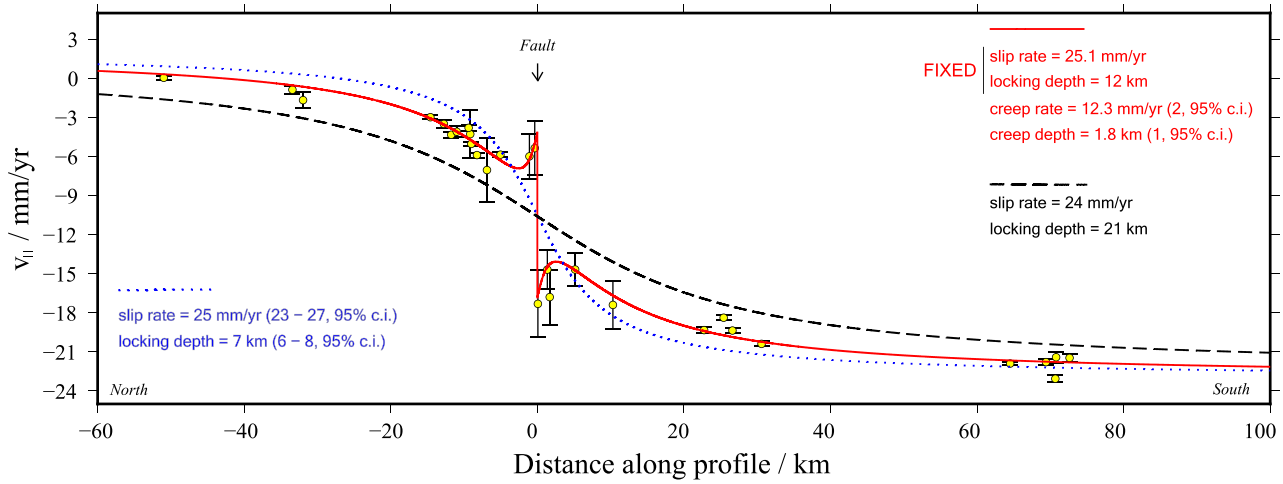

Figure 9. Dashed black and dotted blue lines show McClusky *et al.* (2000) and Ergintav *et al.* (2014) far-field, best fit models in an elastic half-space. Yellow dots are GPS points from this study showing the fault-parallel velocity components. Red is our best fit elastic dislocation model with fixed deep slip rate and locking depth with surface creep near the 1999 Izmit Earthquake epicentre. The fixed and estimated model parameters are shown in top right corner.

fault. It is plausible that such aseismic slip on the deeper levels of the fault could result in more rapid strain accumulation at depths where major earthquakes are expected to nucleate on the Izmit and adjacent unbroken segments, thus advancing the time to the next earthquake (e.g. deep afterslip below the eastern end of the Izmit fault may have triggered the M_w7.2 Duzce Earthquake, e.g. Ergintav *et al.* 2009). In contrast, if the present day, shallow apparent locking depth reflects afterslip that occurs in part at the coseismic (mid- to upper crustal) depths of the fault, afterslip may retard the time to the next earthquake on the Izmit fault. Continuous geodetic monitoring of the space–time evolution of afterslip could improve our understanding of the strain balance between creeping and locked sections along the 1999 rupture zone. Better constraints on afterslip are also essential to estimate the impact on adjacent unbroken fault segments, particularly important are those segments in the Marmara Seismic Gap west of the Izmit rupture (Ergintav *et al.* 2014). As improved observations of post-seismic afterslip become available, classical hazard estimation methods that assume fully locked fault segments should be improved to include space- and time-dependent fault coupling.

5 CONCLUSION

We present an updated GPS velocity field across the central section of the 1999 Izmit rupture including near-fault (within approximately 20 km) and regional (50–70 km) survey and continuous measurements. Survey data consist of five campaigns between 2014 and 2016, and the period of observations from continuous sites varies (2–7 yr) depending on data sources. We report current rates of strain accumulation from GPS velocities across the Izmit coseismic rupture after removing the effects of northwest Anatolia rotation using a local Anatolia–Eurasia Euler vector appropriate for the region south of the Izmit Earthquake segment ($26.692 \pm 0.8^\circ$ N; $31.808 \pm 0.1^\circ$ E; $0{:}84 \pm 0.05^\circ$ Myr^{-1}). Using fault-parallel velocities, and simple elastic half-space models, we estimate the apparent fault locking depth ∼20 yr after the 1999 Earthquake (∼8–12 km); an apparent locking depth that is substantially less than pre-earthquake estimates (∼21 km) indicating that post-seismic processes continue at present. Shallow creep that has been decaying logarithmically with time since the earthquake is highest near the earthquake epicentre (12 mm yr^{-1}; 10–15 mm yr^{-1}, 95 per cent c.i.) and falls off rapidly to the east and west, consistent with previous results of Aslan *et al.* (2019). The low level of seismicity on the fault during the survey period indicates shallow fault creep occurs aseismically. Given the active state and high rates of continuing deformation surrounding the Izmit Earthquake fault, continued and expanded monitoring with focused seismic and geodetic observations offers opportunities to better constrain space–time variations in fault coupling that may provide insights on fault behaviour for other major strike-slip faults such as the San Andreas fault.

ACKNOWLEDGEMENTS

General Directory of Land Registry and Cadaster and the General Directorate of Mapping provided CORS-TR stations RINEX files and Kocaeli General Directorate of Water and Sewerage Administration (ISU), Sakarya General Directorate of Water and Sewerage Administration (SASKI) and Cayirova Municipality provided cGPS RINEX files for this study. We would like to thank Robert King for his help with GPS data processing and analysis, especially the survey observations. We are grateful to Roland Bürgmann and an anonymous reviewer for thorough and constructive reviews that substantially improved the paper. We used GMT for the figures (Wessel *et al.* 2013). MIT participation in this study was supported by a MISTI Grant from MIT. The first author of this paper was also awarded ‘2214-A Abroad Research Scholarship’ by The Scientific and Technological Research Council of Turkey (TUBITAK) and concluded her research at MIT. This study was also supported by TUBITAK 1001 project no. 113Y102 and TUBITAK 2507 project no. 117Y278.

REFERENCES

Ambraseys, N.N., 1970. Some characteristic features of the Anatolian fault zone, *Tectonophysics,*, **9,** 143–165.

Armijo, R., Meyer, B., Barka, A.A., de Chabalier, J.B., Hubert-Ferrari, A. & Cakir, Z., 2000. The fault breaks of the 1999 earthquakes in Turkey and the tectonic evolution of the Sea of Marmara: a summary, in *The 1999 İzmit and Düzce Earthquakes: Preliminary Results,* pp. 55–62, Istanbul Technical University Press, Istanbul: ITU Publication.

Aslan, G., Lasserre, C., Cakir, Z., Ergintav, S., Özarpaci, S., Dogan, U., Bilham, R. & Renard, F., 2019. Shallow creep along the 1999 Izmit Earthquake Rupture (Turkey) from GPS and high temporal resolution interferometric synthetic aperture radar data (2011–2017), *J. geophys. Res.: Solid Earth,* **124,** 2218–2236.

Avouac, J.P., 2015. From geodetic imaging of seismic and aseismic fault slip to dynamic modeling of the seismic cycle, *Annu. Rev. Earth planet. Sci.,* **43,** 233–271.

Barka, A.A., 1996. Slip distribution along the North Anatolian fault associated with the large earthquakes of the period 1939 to 1967, *Bull. seism. Soc. Am.,* **86,** 1238–1254.

Barka, A.A. *et al.*, 2002. The surface rupture and slip distribution of the 17 August 1999 Izmit earthquake (M 7.4), North Anatolian fault, *Bull. seism. Soc. Am.,,* **92,** 43–60.

Bohnhoff, M., Wollin, C., Domigall, D., Küperkoch, L., Martínez-Garzón, P., Kwiatek, G., Dresen, G. & Malin, P.E., 2017. Repeating Marmara Sea earthquakes: indication for fault creep, *Geophys. J. Int.,,* **210**(1), 332–339.

Bondár, I. & Storchak, D.A., 2011. Improved location procedures at the International Seismological Centre, *Geophys. J. Int.,* **186,** 1220–1244.

Bürgmann, R., Schmidt, D., Nadeau, R.M., d'Alessio, M., Fielding, E., Manaker, D., McEvilly, T.V. & Murray, M.H., 2000. Earthquake potential along the northern Hayward fault, California, *Science,* **289**(5482), 1178–1182.

Bürgmann, R., Ergintav, S., Segall, P., Hearn, E.H., McClusky, S., Reilinger, R.E., Woith, H. & Zschau, J., 2002. Time-dependent distributed afterslip on and deep below the Izmit earthquake rupture, *Bull. seism. Soc. Am.,,* **92**(1), 126–137.

Çakir, Z., 2003. *Analysis of the crustal deformation caused by the 1999 İzmit and Düzce earthquakes using Synthetic Aparture Radar Interferometry,* PhD thesis, İstanbul Technical Univ.

Cakir, Z., Chabalier, J.B., Armijo, R., Meyer, B., Barka, A. & Peltzer, G., 2003. Coseismic and early post-seismic slip associated with the 1999 Izmit earthquake (Turkey), from SAR interferometry and tectonic field observations, *Geophys. J. Int.,,* **155**(1), 93–110.

Çakir, Z., Ergintav, S., Özener, H., Dogan, U., Akoglu, A.M., Meghraoui, M. & Reilinger, R., 2012. Onset of aseismic creep on major strike-slip faults, *Geology,,* **40**(12), 1115–1118.

Dong, D., Herring, T.A. & King, R., 1998. Estimating regional deformation from a combination of space and terrestrial geodetic data, *J. Geod.,* **72**(4), 200–214.

Emre, Ö., Duman, T.Y., Özalp, S., Elmacı, H., Ş.Olgun & Şaroğlu, F., 2013. Açıklamalı Türkiye Diri Fay Haritası Ölçek 1/1.125.000, *Maden Tetkik ve Arama Genel Müdürlüğü Özel Yayın Serisi 30. Special Publication Series of MTA-30,* **30,** ISBN: 978-605- 5310-56-1.

Ergintav, S., Burgmann, R., McClusky, S., Çakmak, R., Reilinger, R.E., Lenk, O., Barka, A. & Ozener, H., 2002. Postseismic deformation near the Izmit earthquake (17 August 1999, M 7.5) rupture zone, *Bull. seism. Soc. Am.,,* **92**(1), 194–207.

Ergintav, S., Doğan, U., Gerstenecker, C., Cakmak, R., Belgen, A., Demirel, H., Aydın, C. & Reilinger, R., 2007. A snapshot (2003–2005) of the 3D postseismic deformation for the 1999, Mw = 7.4 Izmit earthquake in the Marmara Region, Turkey, by first results of joint gravity and GPS monitoring, *J. Geodyn.,* **44**(1–2), 1–18.

Ergintav, S. *et al.*, 2009. Seven years of postseismic deformation following the 1999, M= 7.4 and M= 7.2, Izmit-Düzce, Turkey earthquake sequence, *J. geophys. Res.: Solid Earth,* **114**(B7), doi: 10.1029/2008JB006021.

Ergintav, S. *et al.*, 2014. Istanbul's earthquake hot spots: geodetic constraints on strain accumulation along faults in the Marmara seismic gap, *Geophys. Res. Lett.,,* **41**(16), 5783–5788.

Feigl, K.L. *et al.*, 2002. Estimating slip distribution for the Izmit mainshock from coseismic GPS, ERS-1, RADARSAT, and SPOT measurements, *Bull. seism. Soc. Am.,,* **92**(1), 138–160.

Floyd, M.A. & Herring, T.A., 2020. *Geodetic Time Series Analysis in Earth Sciences,* Springer, pp. 157–183.

Hearn, E.H., Bürgmann, R. & Reilinger, R.E., 2002. Dynamics of Izmit earthquake postseismic deformation and loading of the Duzce earthquake hypocenter, *Bull. seism. Soc. Am.,,* **92**(1), 172–193.

Hearn, E.H., McClusky, S., Ergintav, S. & Reilinger, R.E., 2009. Izmit earthquake postseismic deformation and dynamics of the North Anatolian Fault Zone, *J. geophys. Res.: Solid Earth,* **114**(B8), doi: 10.1029/2008JB006026.

Herring, T.A., King, R.W., Floyd, M.A. & McClusky, S.C., 2018. *Introduction to GAMIT/GLOBK, Release 10.7,* Cambridge. Department of Earth, Atmospheric, and Planetary Sciences, Massachusetts Institute of Technology, USA. Available at: http://geoweb.mit.edu/gg/Intro_GG.pdf.

Hussain, E., Wright, T.J., Walters, R.J., Bekaert, D., Hooper, A. & Houseman, G.A, 2016a. Geodetic observations of postseismic creep in the decade after the 1999 Izmit earthquake, Turkey: implications for a shallow slip deficit, *J. geophys. Res.: Solid Earth,* **121**(4), 2980–3001.

Hussain, E., Hooper, A., Wright, T.J., Walters, R.J. & Bekaert, D.PS., 2016b. Interseismic strain accumulation across the central North Anatolian Fault from iteratively unwrapped InSAR measurements, *J. geophys. Res.: Solid Earth,* **121**(12), 9000–9019.

International Seismological Centre, 2018. *On-line bulletin*. Available at: https://doi.org/10.31905/D808B830. (accessed December 8, 2018).

Lorenzo-Martín, F., Roth, F. & Wang, R., 2006. Elastic and inelastic triggering of earthquakes in the North Anatolian Fault zone, *Tectonophysics,,* **424,** 271–289.

McClusky, S. *et al.*, 2000. Global Positioning System constraints on plate kinematics and dynamics in the eastern Mediterranean and Caucasus, *J. geophys. Res.: Solid Earth,* **105,** 5695–5719.

Nalbant, S.S., Hubert, A. & King, G.C., 1998. Stress coupling between earthquakes in northwest Turkey and the north Aegean Sea, *J. geophys. Res.: Solid Earth,* **103,** 24469–24486.

Parsons, T., 2004. Recalculated probability of $M \geq 7$ earthquakes beneath the Sea of Marmara, Turkey, *J. geophys. Res.: Solid Earth,* **109**(B5), doi: 10.1029/2003JB002667.

Reilinger, R. *et al.*, 2000. Coseismic and postseismic fault slip for the 17 August 1999, M= 7.5, Izmit, Turkey earthquake, *Science,* **289**(5484), 1519–1524.

Reilinger, R. *et al.*, 2006. GPS constraints on continental deformation in the Africa-Arabia-Eurasia continental collision zone and implications for the dynamics of plate interactions, *J. geophys. Res.: Solid Earth,* **111**(B5), doi: 10.1029/2005JB004051.

Savage, J.C. & Burford, R.O., 1973. Geodetic determination of relative plate motion in central California, *J. geophys. Res.,,* **78**(5), 832–845.

Savage, J.C., 1990. Equivalent strike-slip earthquake cycles in half-space and lithosphere-asthenosphere earth models, *J. geophys. Res.: Solid Earth,* **95**(B4), 4873–4879.

Smith-Konter, B.R., Sandwell, D.T. & Shearer, P., 2011. Locking depths estimated from geodesy and seismology along the San Andreas Fault System: implications for seismic moment release, *J. geophys. Res.: Solid Earth,* **116**(B6), doi: 10.1029/2010JB008117.

Stein, R.S., Barka, A.A. & Dieterich, J.H., 1997. Progressive failure on the North Anatolian fault since 1939 by earthquake stress triggering, *Geophys. J. Int.,,* **128,** 594–604.

Straub, C., Kahle, H.G. & Schindler, C., 1997. GPS and geologic estimates of the tectonic activity in the Marmara Sea region, NW Anatolia, *J. geophys. Res.: Solid Earth,* **102,** 27587–27601.

Şengör, A.M.C., Tüysüz, O., Imren, C., Sakınç, M., Eyidoğan, H., Görür, N., Le Pichon, X. & Rangin, C., 2005. The North Anatolian fault: a new look, *Annu. Rev. Earth Planet. Sci.,* **33,** 37–112.

Toksöz, M.N., Reilinger, R.E., Doll, C.G., Barka, A.A. & Yalcin, N., 1999. Izmit (Turkey) earthquake of 17 August 1999: first report, *Seismol. Res. Lett.,* **70,** 669–679.

Wang, L., Wang, R., Roth, F., Enescu, B., Hainzl, S. & Ergintav, S., 2009. Afterslip and viscoelastic relaxation following the 1999 M 7.4 Izmit earthquake from GPS measurements, *Geophys. J. Int.,,* **178**(3), 1220–1237.

Wessel, P., Smith, W.H.F., Scharroo, R., Luis, J. & Wobbe, F., 2013. Generic mapping tools: improved version released, *EOS, Trans. Am. geophys. Un.,* **94**(45), 409–410.

Wright, T., Fielding, E. & Parsons, B., 2001. Triggered slip: observations of the 17 August 1999 Izmit (Turkey) earthquake using radar interferometry, *Geophys. Res. Lett.,,* **28**(6), 1079–1082.

Yamasaki, T., Wright, T.J. & Houseman, G.A., 2014. Weak ductile shear zone beneath a major strike-slip fault: inferences from earthquake cycle model constrained by geodetic observations of the western North Anatolian Fault Zone, *J. geophys. Res.: Solid Earth,* **119**(4), 3678–3699.

Zabcı, C., 2019. Spatio-temporal behaviour of continental transform faults: implications from the late Quaternary slip history of the North Anatolian Fault, Turkey, *Can. J. Earth Sci.,* **56**(11), 1218–1238.

SUPPORTING INFORMATION

Supplementary data are available at *GJI* online.

Table S1. GPS stations derived velocities. No: number of campaigns, c used for continuous stations, Lat: Latitude (N°), Long: Longitude (E°), T_1: time of first data processed, T_2: time of last data processed, Time: data processed in years, v_e: East velocity, v_n: North velocity, σ_{ve}: standard deviation for east velocity, and σ_{vn}: standard deviation for north velocity.

Figure S1. Map showing GPS sites used to estimate the regional Anatolian Euler Vector for the Izmit-Marmara region and active faults (black lines, Emre *et al.* 2013).

Figure S2. (a) Reilinger *et al.* (2006) GPS velocities, 1999 Izmit rupture (orange lines) and active faults (black lines, Emre *et al.* 2013), (b) fault-normal velocities and (c) fault-parallel velocities.

Figure S3. 20 yr velocity map of 1999 Izmit rupture area. Blue, red and black arrows show velocity fields of McClusky *et al.* (2000) and Ergintav *et al.* (2014) and this study, respectively, with 95 per cent confidence ellipses relative to Eurasia, 1999 Izmit rupture (orange lines) and active faults (black lines, Emre *et al.* 2013).

Please note: Oxford University Press is not responsible for the content or functionality of any supporting materials supplied by the authors. Any queries (other than missing material) should be directed to the corresponding author for the paper.